Strong Local Evaporative Cooling Over Land Due to Atmospheric Aerosols – Supplementary Information

TC Chakraborty[1*], Xuhui Lee[1], and David M. Lawrence[2]

[1]School of the Environment, Yale University, New Haven, CT, USA

[2]National Center for Atmospheric Research, Boulder, CO, USA

Corresponding Author: TC Chakraborty (tc.chakraborty@yale.edu)

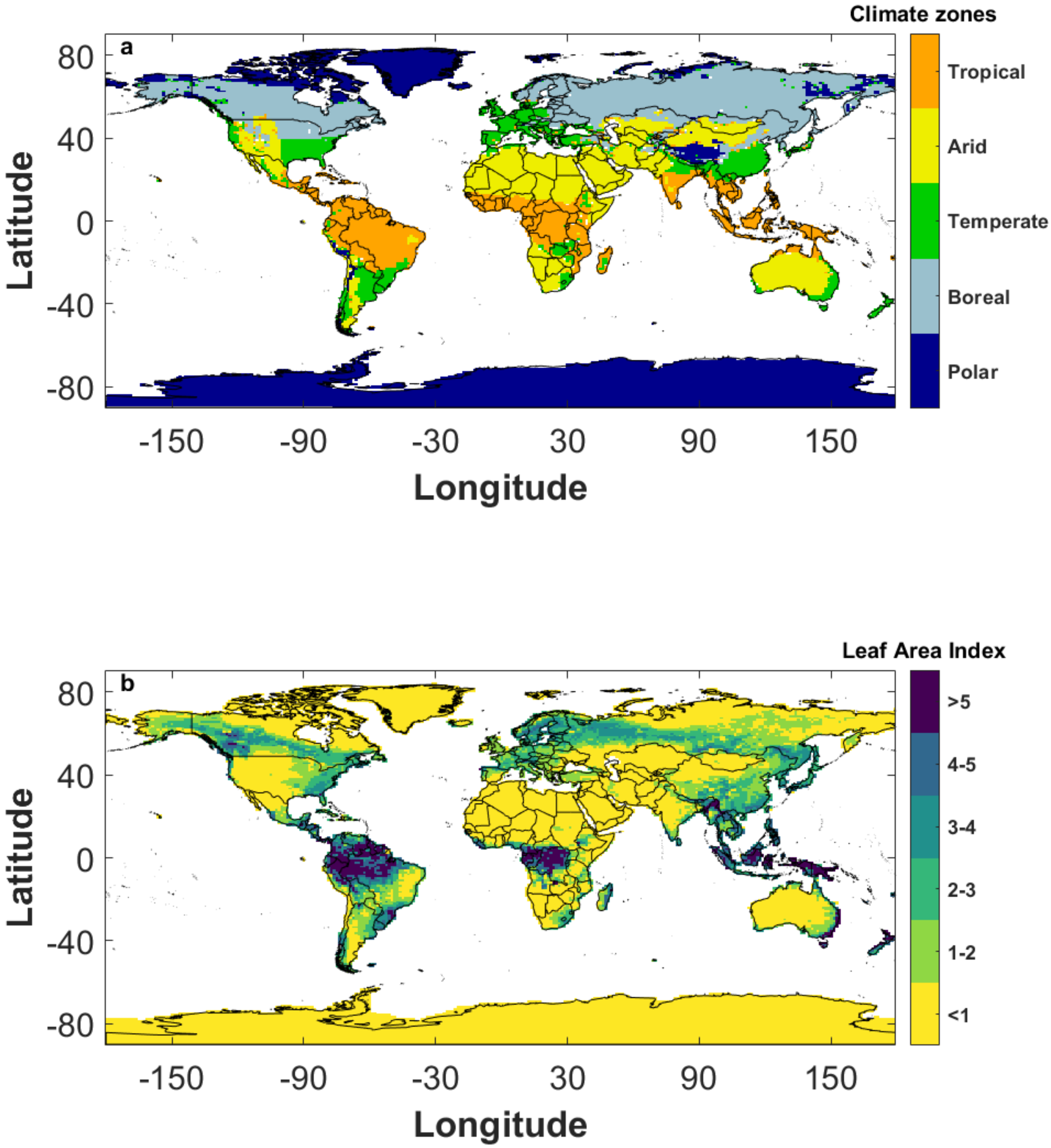

Figure S1. Maps of study area. Global distribution of **a** Koppen-Geiger climate zones and **b** leaf area index (LAI) bins.

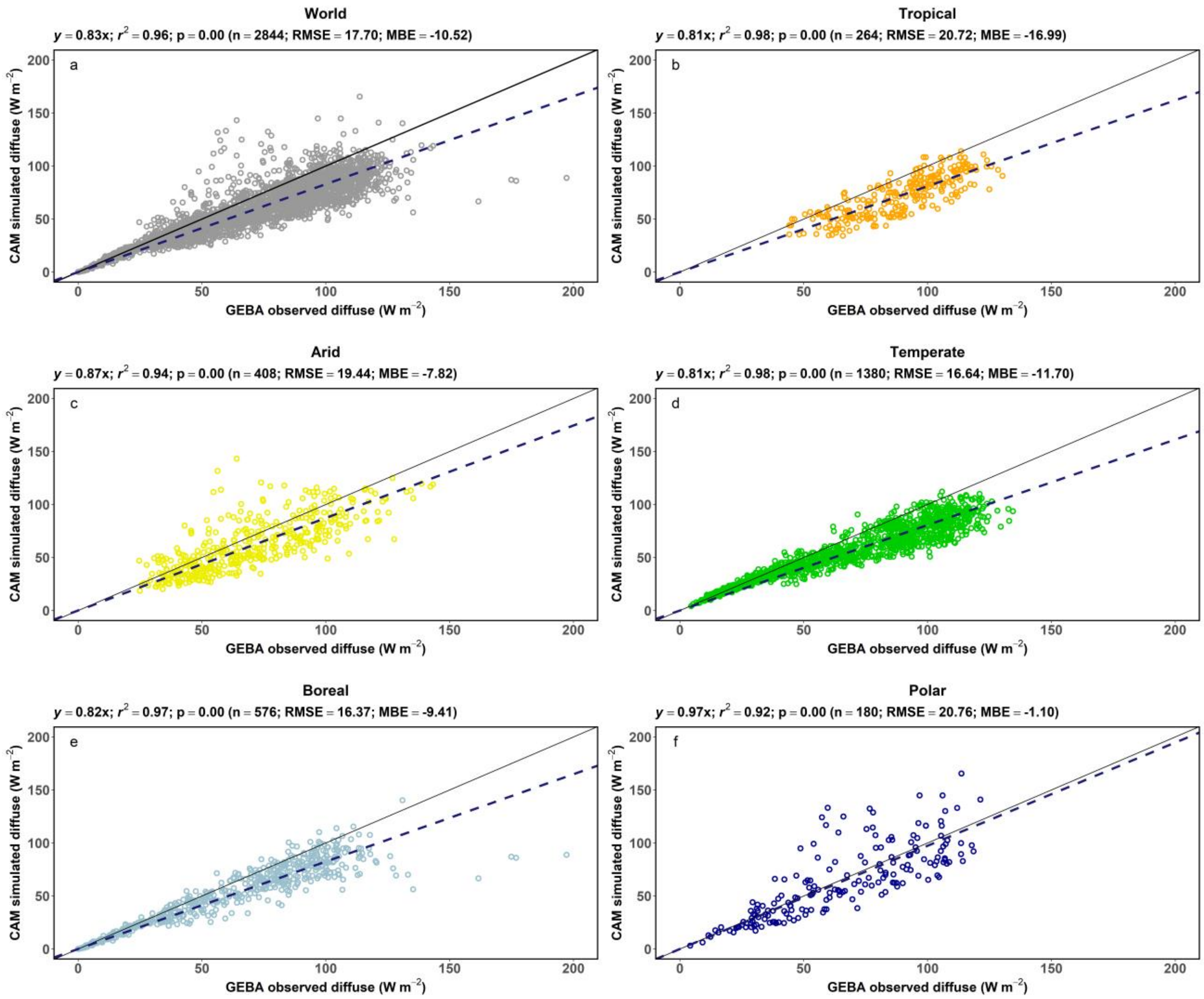

Figure S2. Evaluation of diffuse radiation. Grid-level evaluation of monthly incoming diffuse radiation at surface from the CAM run against GEBA observations for **a** all sites, **b** tropical sites, **c** arid sites, **d** temperate sites, **e** boreal sites, and **f** polar sites.

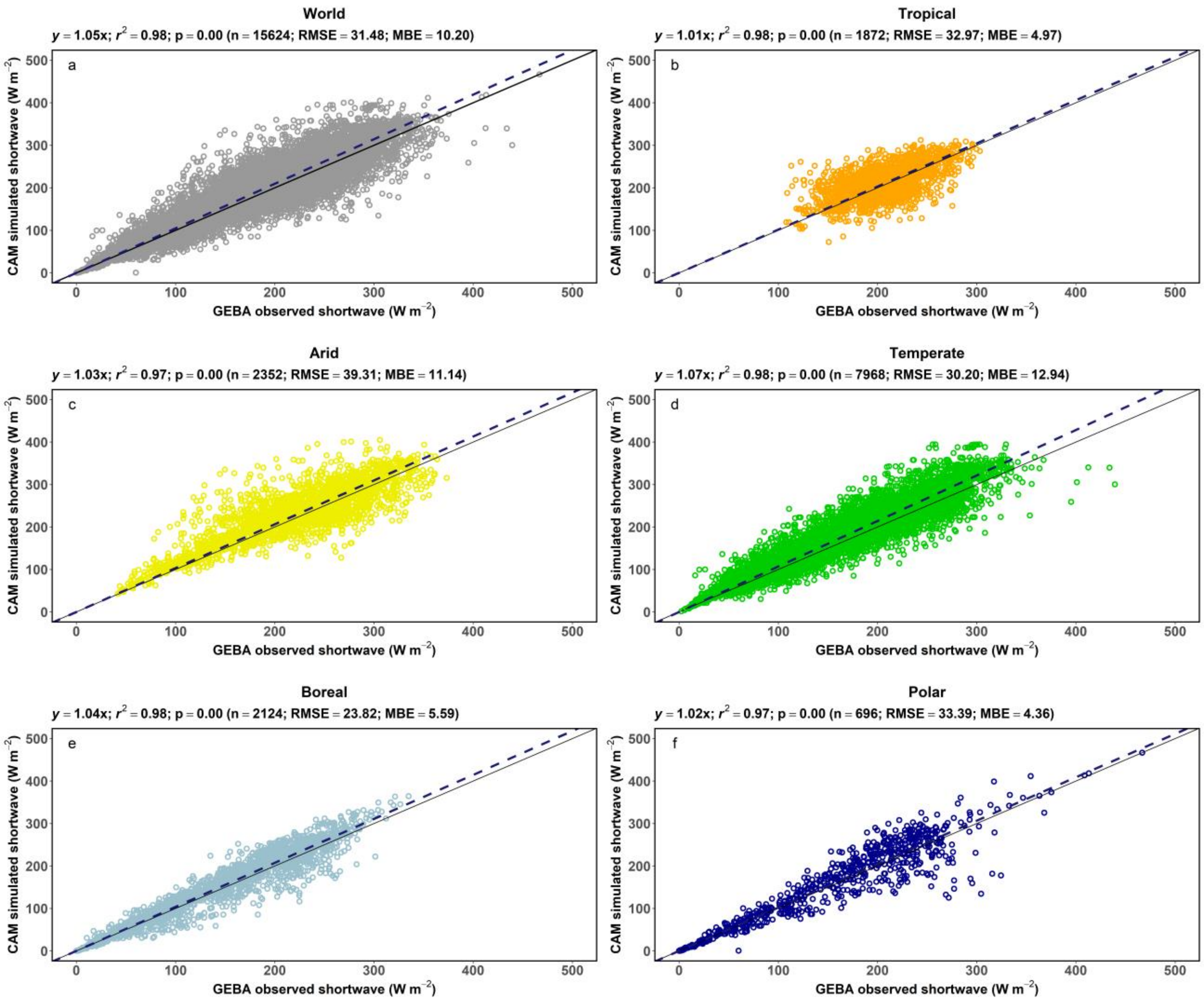

Figure S3. Evaluation of shortwave radiation. Grid-level evaluation of monthly incoming shortwave radiation at surface from the CAM run against GEBA observations for **a** all sites, **b** tropical sites, **c** arid sites, **d** temperate sites, **e** boreal sites, and **f** polar sites.

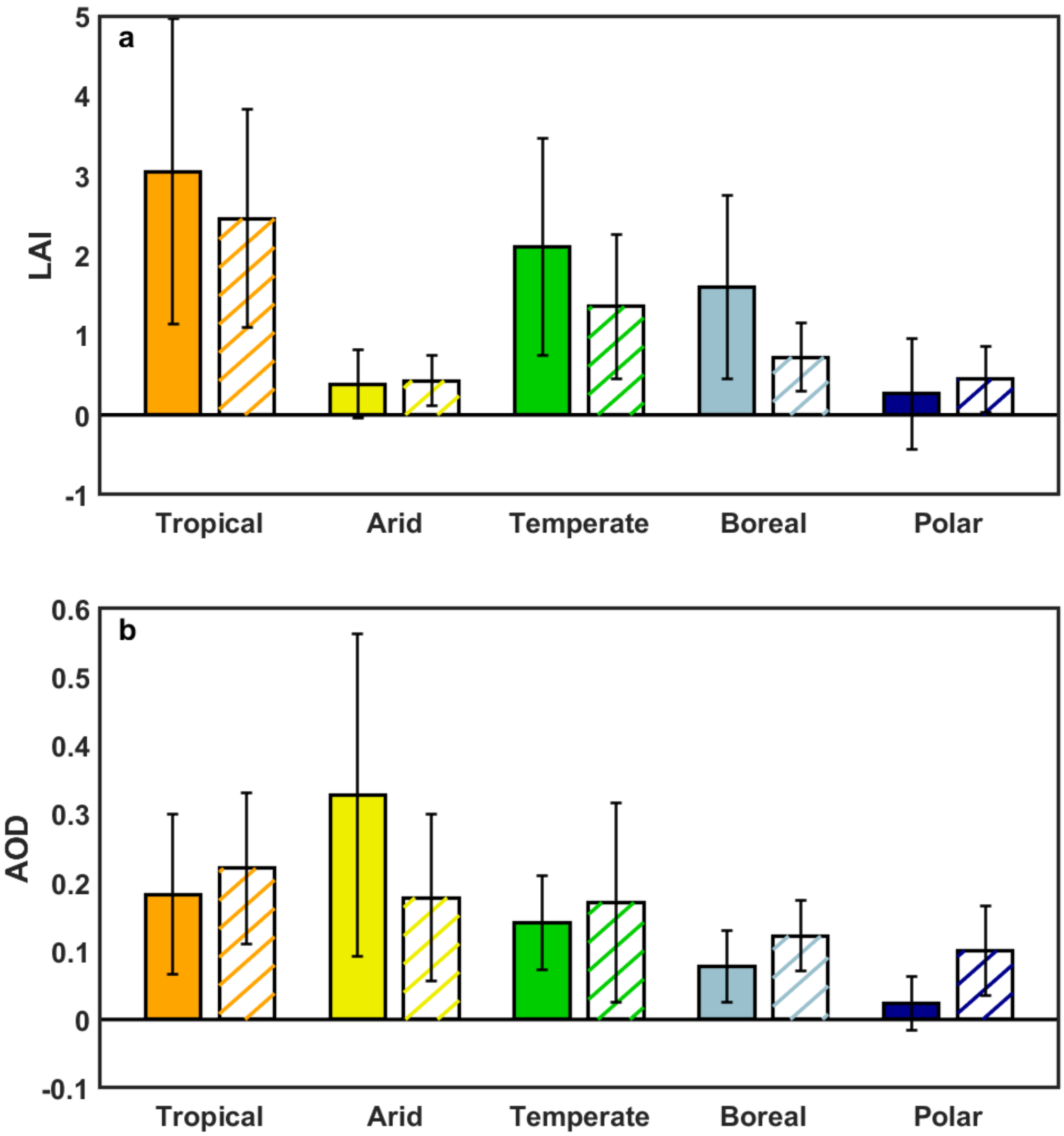

Figure S4. Comparison of leaf area index (LAI) and aerosol optical depth (AOD) with satellite observations. Grid-area weighted mean (bars) and standard deviation (error bars) of LAI and AOD from our CLM and CAM runs compared with 5-year averages (2003-2007) observed by satellites for each climate zone are shown. The filled bars are for the parameters in the models, while the hatched bars represent the satellite observations.

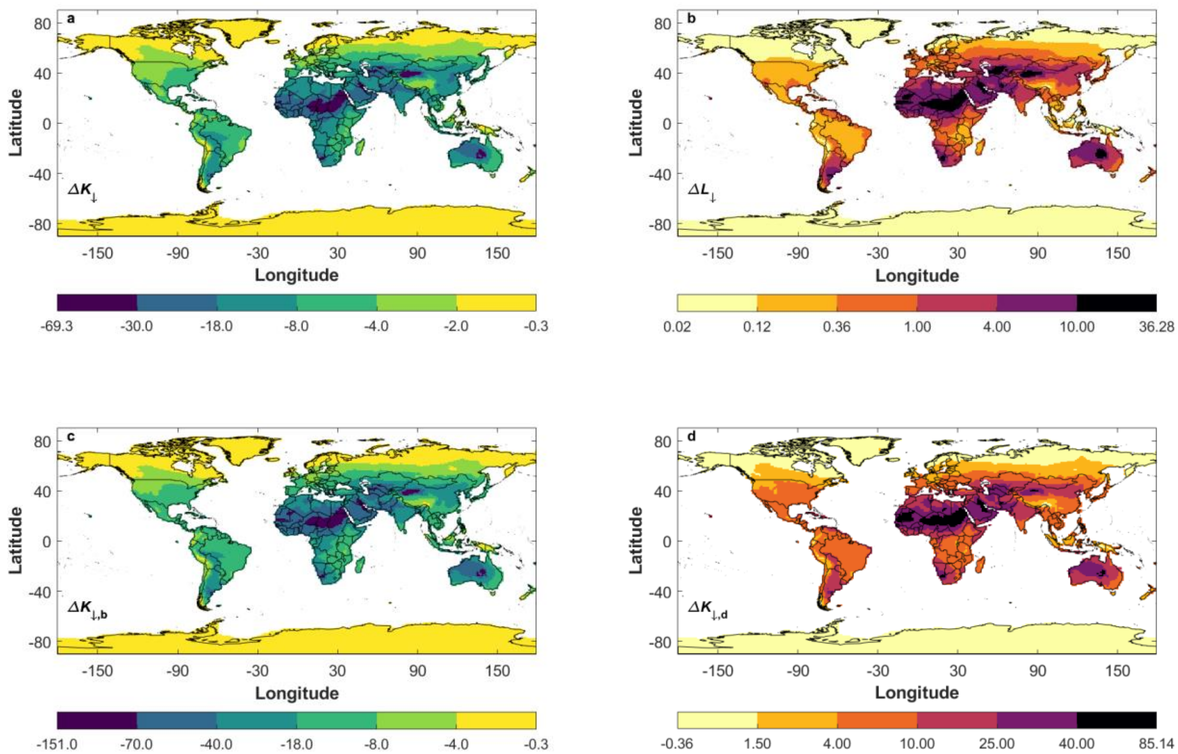

Figure S5. Global patterns of changes in incoming radiation at the surface due to aerosols. Global maps of **a**, shortwave radiative effect ($\Delta K_{\downarrow}$), **b** longwave radiative effect ($\Delta L_{\downarrow}$), **c** change in beam radiation ($\Delta K_{\downarrow,b}$), and **d** change in diffuse radiation ($\Delta K_{\downarrow,d}$). All quantities are in W m^{-2}. Non-linear color scales are used to better visualize the spatial variations.

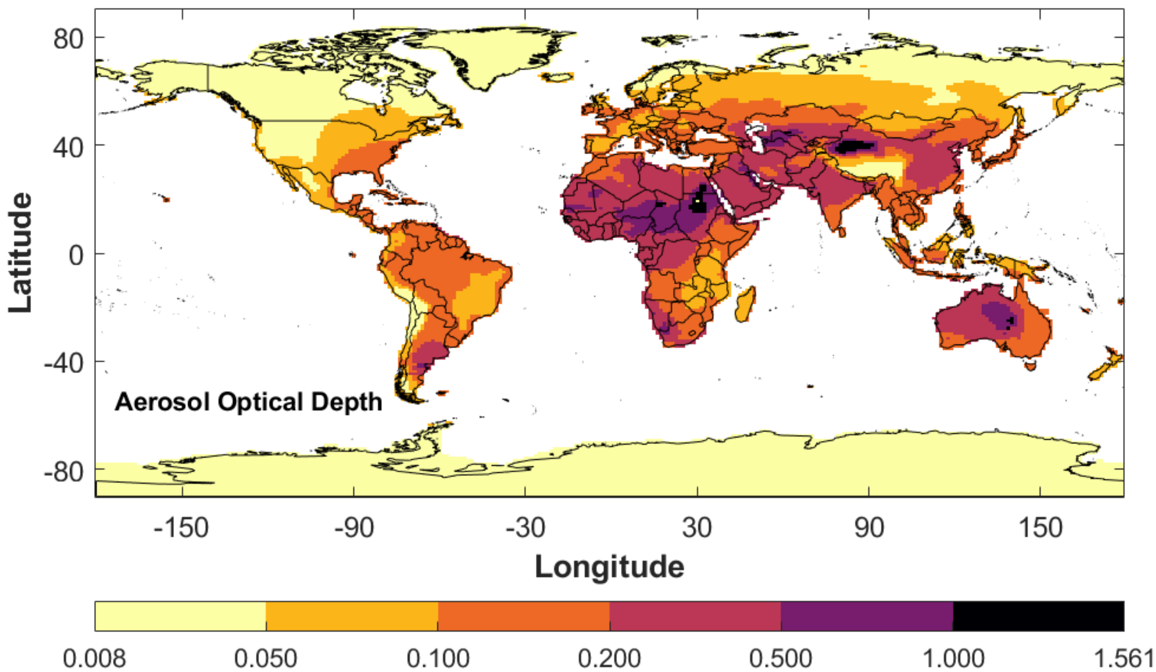

Figure S6. Global patterns of aerosol optical depth. Non-linear color scales are used to better visualize the spatial variations.

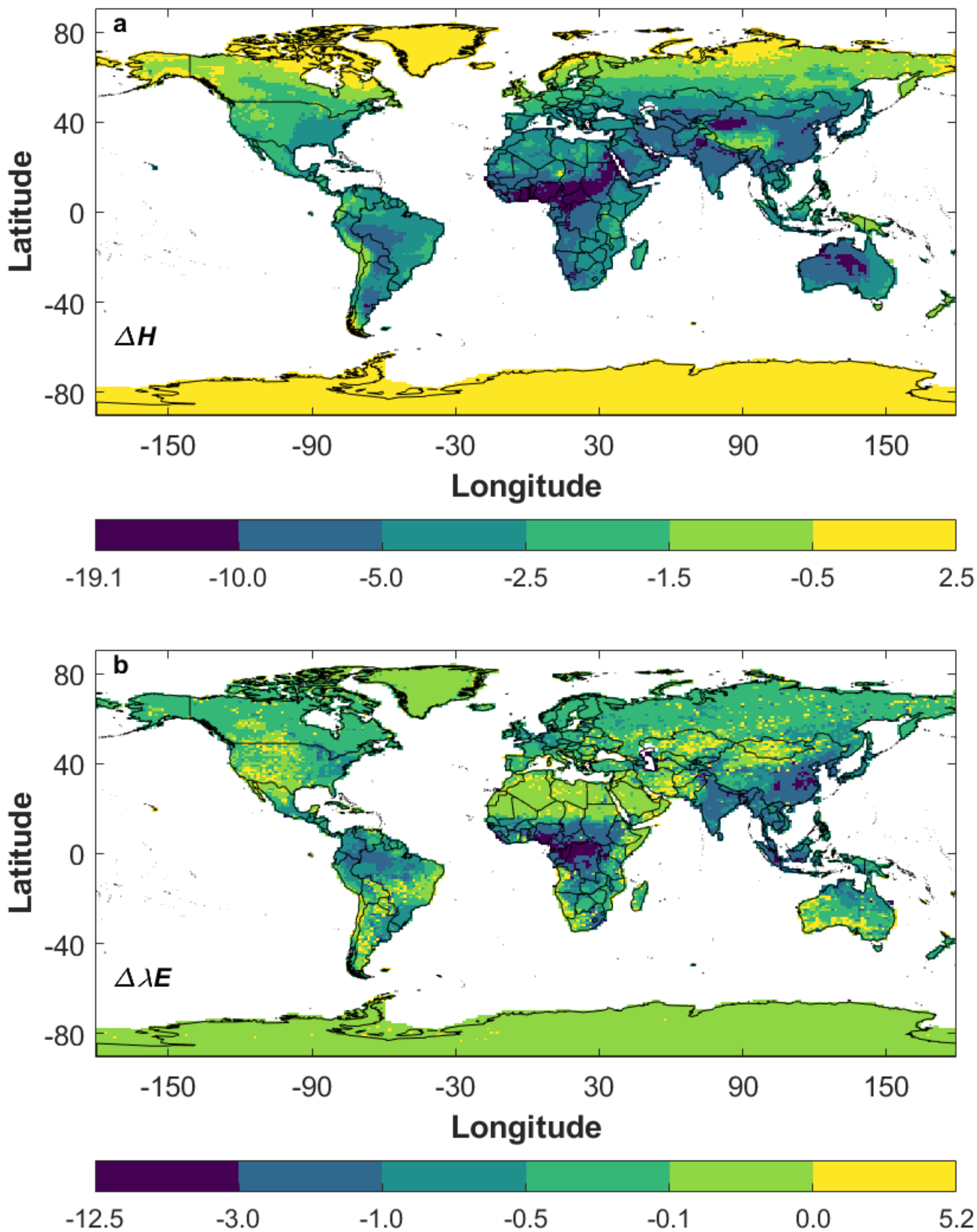

Figure S7. Global patterns of changes in turbulent fluxes due to aerosols. Global maps of **a**, change in sensible heat flux (ΔH), and **b** change in latent heat flux ($\Delta\lambda E$). All values are in W m^{-2}. Non-linear color scales are used to better visualize the spatial variations.

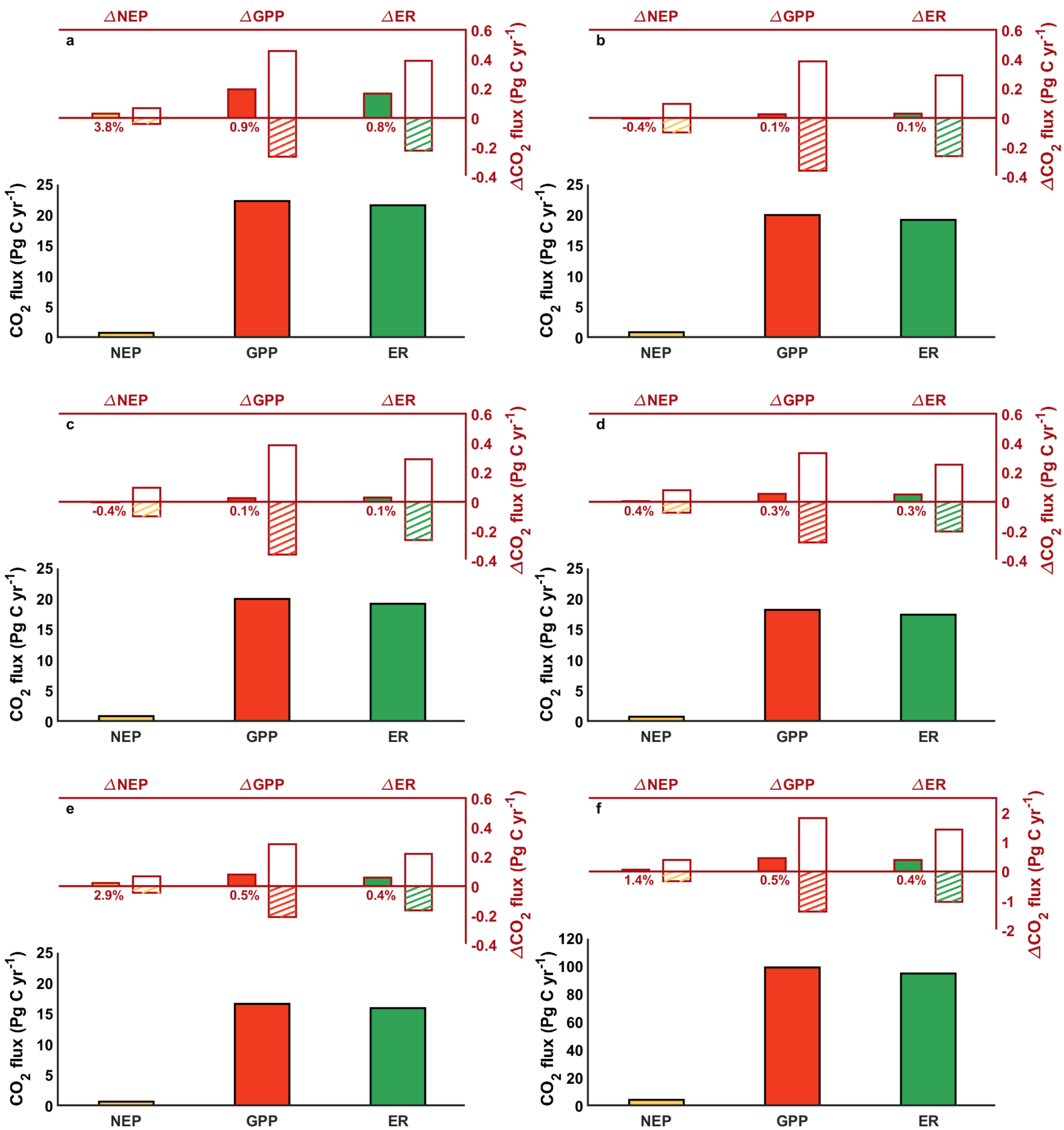

Figure S8. Carbon budget across vegetation density zones. Net ecosystem production (NEP, orange bar), gross primary productivity (GPP, red bar), and ecosystem respiration (ER , green bar) over **a** grids with leaf area index (LAI) <1, **b** between 1 to 2, **c** between 2 to 3, **d** between 3 to 4, **e** between 4 to 5, and **f** and above 5. The carbon flux components for a clean atmosphere are represented by the filled bars in the lower part of each panel. The net changes due to aerosols are given by the filled bars in the upper part of the panel, with the percentage changes noted. The net changes are further decomposed into contributions from the diffuse radiation fertilization effect (blank bar) and the dimming effect (hatched bar).

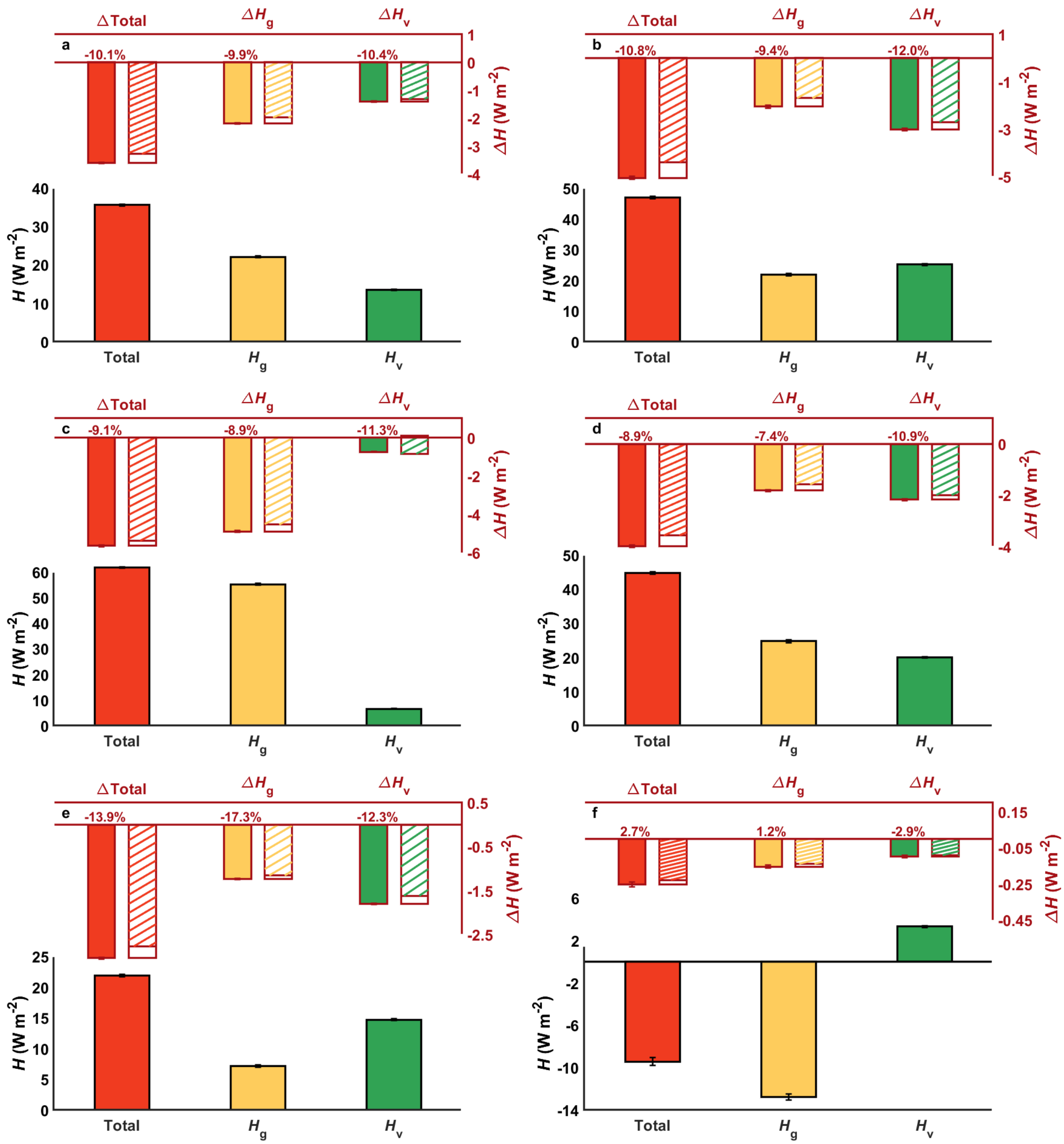

Figure S9. Components of sensible heat flux across climate zones. Total grid area-weighted mean sensible heat flux (H, red bar), sensible heat flux from ground (H_g, orange bar), and sensible heat flux from vegetation (H_v, green bar) over **a** all terrestrial surfaces, **b** tropical climate, **c** arid climate, **d** temperate climate, **e** boreal climate, and **f** polar climate. The components for the clean atmosphere are represented by the filled bars in the lower part of each panel. The net changes due to aerosols are given by the filled bars in the upper part of the panel, with the percentage changes noted. The net changes are further decomposed into contributions from the diffuse radiation fertilization effect (blank bar) and the dimming effect (hatched bar). The error bars represent the grid area-weighted standard errors.

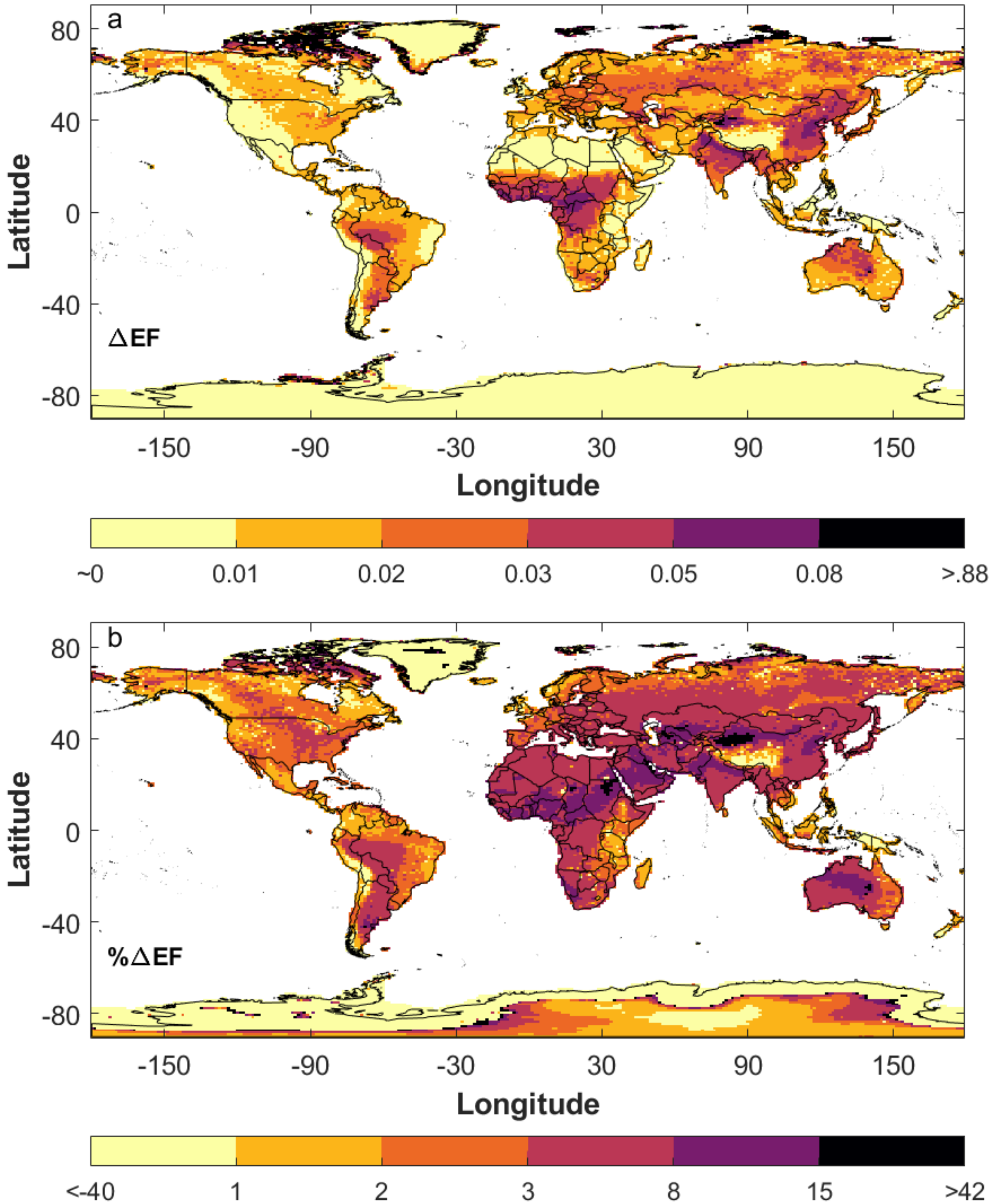

Figure S10. Global patterns of changes in evaporative fraction due to aerosols. Global maps of **a** change in evaporative fraction (ΔEF; unitless) and **b** percentage change in evaporative fraction

(%ΔEF). The global mean ΔEF and %ΔEF are 0.023 and 4.5%, respectively. Non-linear color scales are used to better visualize the spatial variations.

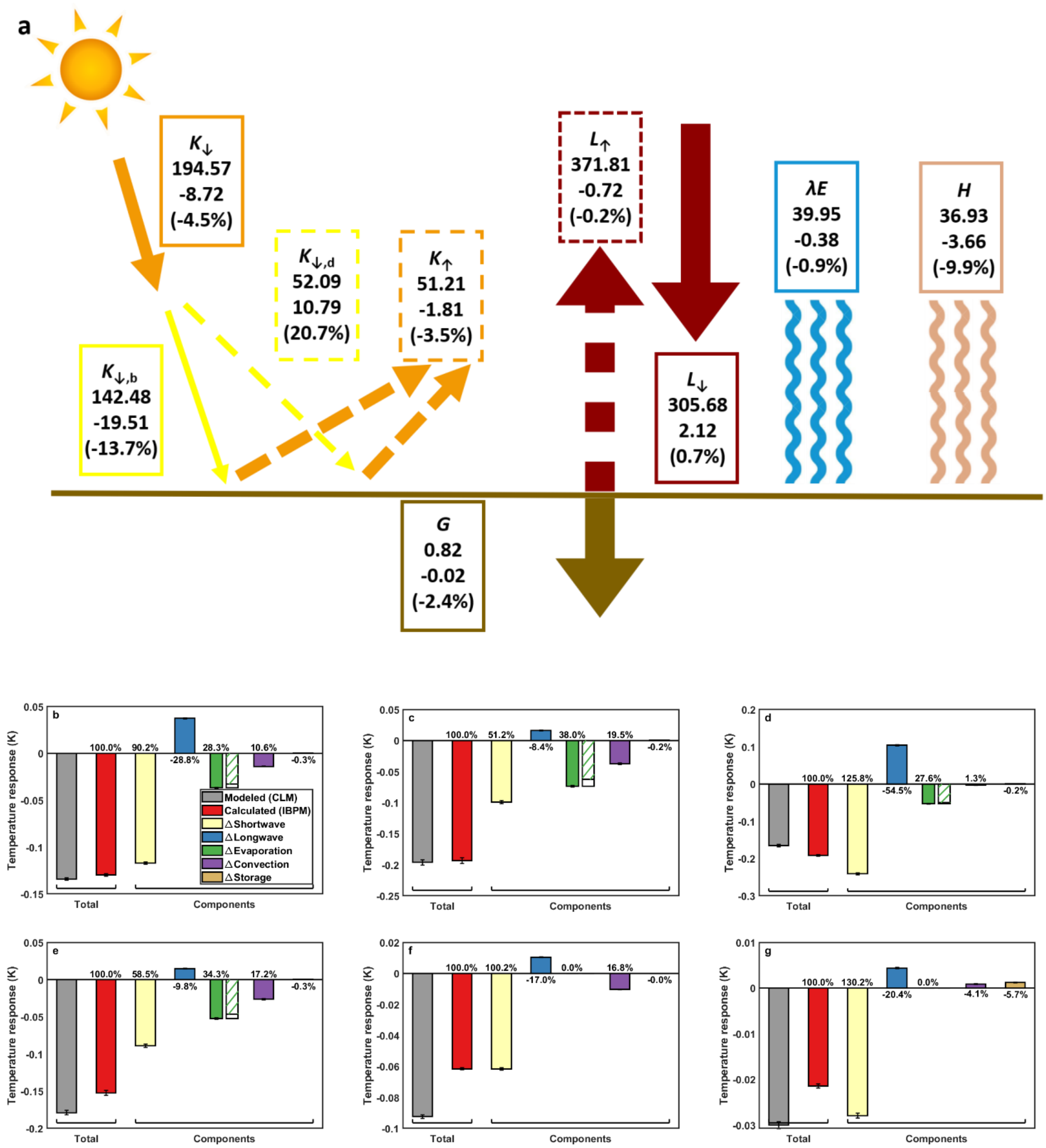

Figure S11. Examining consistency of results using CLM4.5. Identical to Fig. 3 and Fig. 7 of main text but using CLM4.5 results instead of CLM5.0.

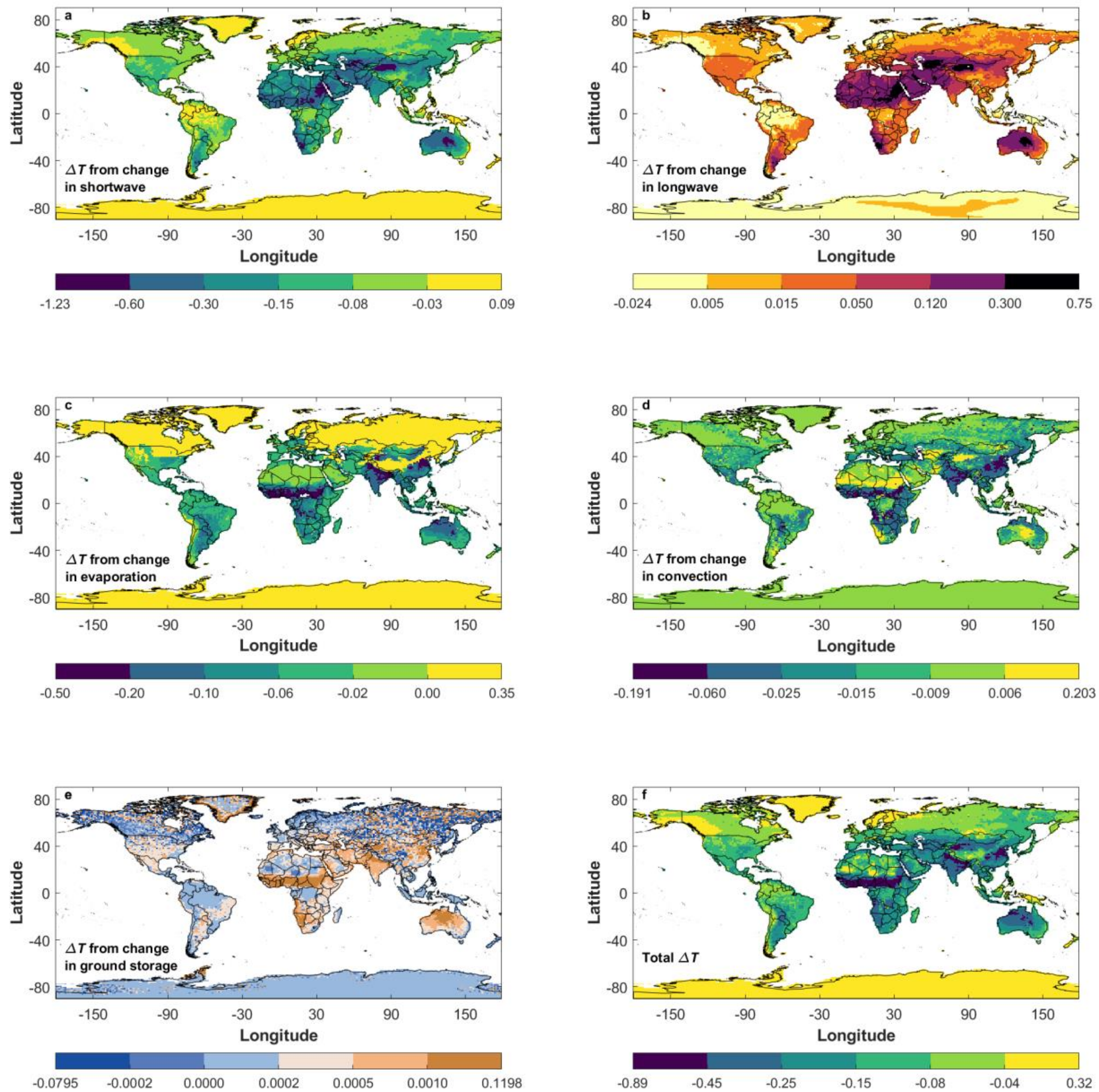

Figure S12. Global patterns of different pathways of aerosol-induced temperature response. Global maps of local temperature response (K) from **a** aerosol shortwave radiative effect at surface, **b** aerosol longwave radiative effect at surface, **c** aerosol-induced evaporation change, **d** aerosol-induced convection change, **e** aerosol-induced ground storage change, and **f** the sum of all pathways. Non-linear color scales are used to better visualize the spatial variations.

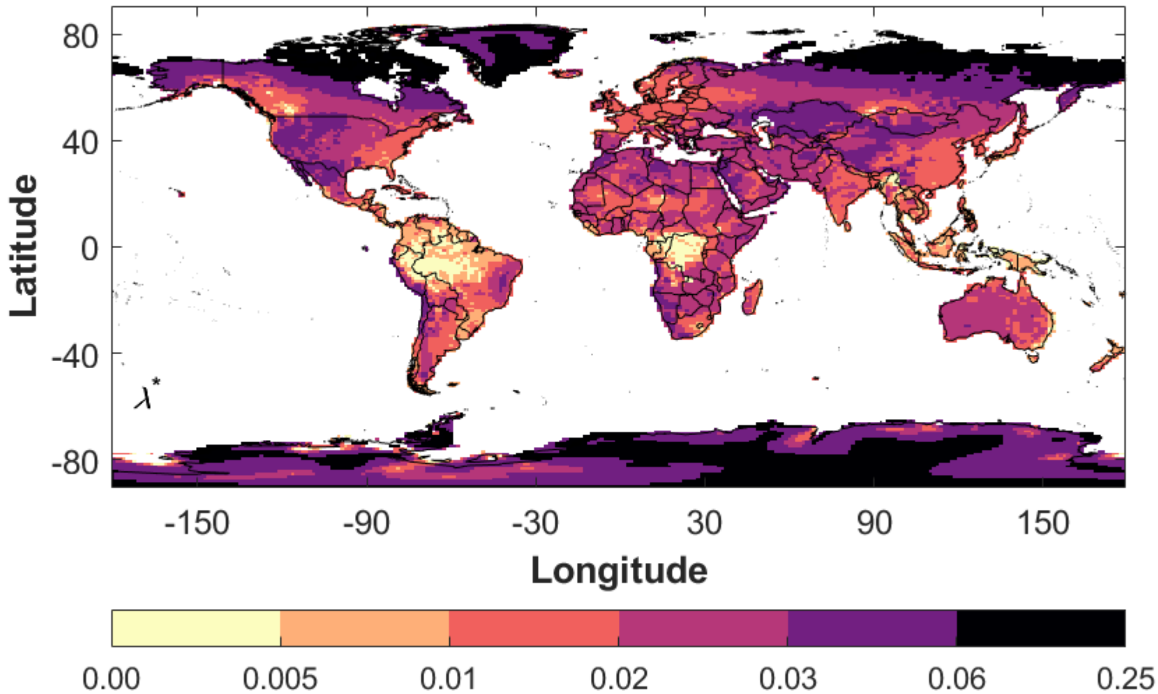

Figure S13. Global patterns of effective local climate sensitivity. Values are in K W^{-1} m^2. Non-linear color scales are used to better visualize the spatial variations.

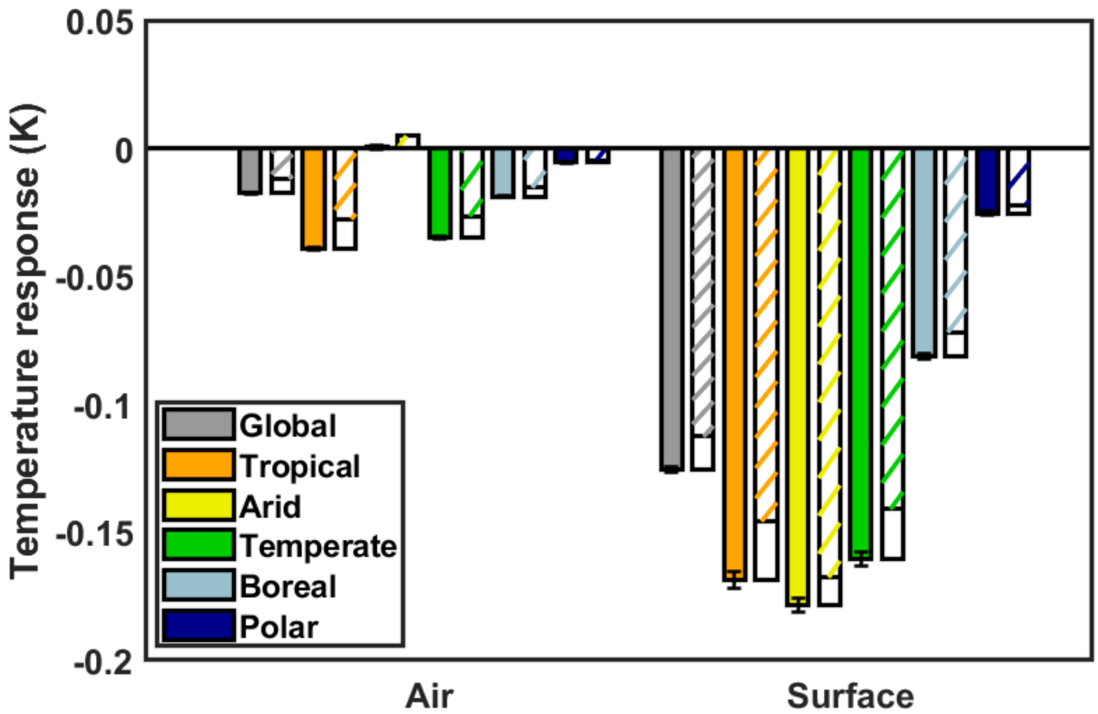

Figure S14. Surface and air temperature response to aerosols for all land surfaces and each climate zone. The filled bars represent the net changes. These changes are further decomposed into contributions from the diffuse radiation fertilization effect (blank bar) and the dimming effect (hatched bar). The error bars represent the grid area-weighted standard errors.

Table S1. Summary of grid area-weighted annual mean components of the surface radiation energy budgets from CAM and CLM runs for aerosol and no aerosol cases, as well as their changes, for the world's land surface and for each climate zone.

		Regions of interest					
Variable	**Case**	**Global land**	**Tropical**	**Arid**	**Temperate**	**Boreal**	**Polar**
Incoming shortwave ($W\ m^{-2}$)	**Without aerosols**	194.57 ± 59.62	216.35 ± 22.24	257.45 ± 28.76	198.13 ± 33.14	139.83 ± 42.85	140.63 ± 43.72
	With aerosols	185.85 ± 54	206.8 ± 21.14	240.06 ± 26.26	190.4 ± 31.93	135.95 ± 40.55	139.4 ± 42.71
	Change	-8.72 ± 8.98	-9.55 ± 6.76	-17.39 ± 10.65	-7.74 ± 4.55	-3.88 ± 3.17	-1.23 ± 1.99
Reflected shortwave ($W\ m^{-2}$)	**Without aerosols**	50.85 ± 32.02	31.68 ± 4.83	64.88 ± 30.47	30.24 ± 7.61	33.35 ± 13.02	94.25 ± 32.3
	With aerosols	49.08 ± 31.05	30.58 ± 4.58	60.46 ± 27.87	29.22 ± 7.33	32.73 ± 12.78	93.78 ± 32.25
	Change	-1.77 ± 2.62	-1.1 ± 0.93	-4.42 ± 3.79	-1.02 ± 0.71	-0.62 ± 0.56	-0.47 ± 0.38
Incoming direct beam ($W\ m^{-2}$)	**Without aerosols**	142.48 ± 63.66	148.53 ± 30.55	214.96 ± 33.6	147.13 ± 36.81	89.49 ± 44.58	88.58 ± 46.17
	With aerosols	122.97 ± 49.93	129.53 ± 27.59	172.58 ± 28.3	131.33 ± 32.76	81.94 ± 39.21	85.97 ± 44.14
	Change	-19.51 ± 20.81	-19 ± 12.62	-42.38 ± 24.05	-15.8 ± 8.46	-7.55 ± 6.78	-2.61 ± 4.02
Incoming diffuse ($W\ m^{-2}$)	**Without aerosols**	52.09 ± 13.35	67.82 ± 10.09	42.49 ± 8.97	51.01 ± 10.16	50.34 ± 7.29	52.05 ± 15.01
	With aerosols	62.88 ± 14.3	77.27 ± 9.13	67.48 ± 13.63	59.07 ± 8.59	54.01 ± 6.66	53.43 ± 15.3
	Change	10.79 ± 12.22	9.45 ± 6.33	24.99 ± 14	8.06 ± 4.59	3.67 ± 3.7	1.38 ± 2.07
Incoming longwave ($W\ m^{-2}$)	**Without aerosols**	305.68 ± 78.83	395.8 ± 16.39	328.73 ± 38.39	338.06 ± 27.78	270.37 ± 21.66	174.98 ± 62.26
	With aerosols	307.8 ± 79.7	396.95 ± 16.1	334.71 ± 39.37	339.08 ± 27.56	270.9 ± 21.82	175.13 ± 62.36
	Change	2.12 ± 3.73	1.16 ± 1.84	5.98 ± 5.18	1.02 ± 1.14	0.53 ± 0.82	0.14 ± 0.6
Emitted longwave ($W\ m^{-2}$)	**Without aerosols**	375.03 ± 89.73	452.02 ± 13.36	434.74 ± 38.39	408.34 ± 27.46	324.52 ± 31.73	222.39 ± 63.39
	With aerosols	374.32 ± 89.33	451 ± 12.96	433.69 ± 38.26	407.43 ± 27.1	324.13 ± 31.48	222.28 ± 63.27
	Change	-0.72 ± 0.77	-1.03 ± 0.88	-1.05 ± 0.87	-0.91 ± 0.69	-0.4 ± 0.38	-0.11 ± 0.2
Sensible heat flux ($W\ m^{-2}$)	**Without aerosols**	35.64 ± 29.7	46.94 ± 14.24	61.85 ± 15.51	44.78 ± 14.65	21.86 ± 13.24	-9.43 ± 25.45
	With aerosols	32.05 ± 27.86	41.87 ± 14.22	56.22 ± 14.96	40.78 ± 14.59	19.89 ± 12.27	-9.82 ± 24.86
	Change	-3.59 ± 3.03	-5.08 ± 2.97	-5.64 ± 2.95	-4 ± 2.08	-1.97 ± 1.46	-0.39 ± 0.86
Latent heat flux ($W\ m^{-2}$)	**Without aerosols**	37.93 ± 29.68	81.5 ± 17.39	24.45 ± 17.82	52.42 ± 17.14	28.24 ± 10.85	7.3 ± 11.33
	With aerosols	37.42 ± 29.23	80.33 ± 17.13	24.18 ± 17.52	51.66 ± 16.8	27.9 ± 10.68	7.19 ± 11.17
	Change	-0.51 ± 0.8	-1.16 ± 1.13	-0.27 ± 0.57	-0.77 ± 0.85	-0.35 ± 0.39	-0.11 ± 0.23
Ground flux ($W\ m^{-2}$)	**Without aerosols**	0.8 ± 1.43	0 ± 0.13	0.26 ± 0.5	0.44 ± 0.87	2.24 ± 1.54	1.11 ± 2.04
	With aerosols	0.79 ± 1.43	-0.03 ± 0.12	0.24 ± 0.5	0.42 ± 0.87	2.24 ± 1.54	1.1 ± 2.03
	Change	-0.01 ± 0.03	-0.02 ± 0.02	-0.02 ± 0.02	-0.02 ± 0.02	-0.01 ± 0.04	-0.01 ± 0.04
Imbalance ($W\ m^{-2}$)	**Without aerosols**	-0.01 ± 0.03	0 ± 0	0 ± 0.01	-0.02 ± 0.05	-0.01 ± 0.04	0 ± 0.01
	With aerosols	0 ± 0	0 ± 0	0 ± 0	0 ± 0	0 ± 0	0 ± 0
	Change	0 ± 0	0 ± 0	0 ± 0	0 ± 0	0 ± 0	0 ± 0

Table S2. Evaluation of the forcing fields from our CAM run against GSWP3 for the period 2001-2003 for the world's land surfaces and for each climate zones. The top two rows for each variable show the grid-area weighted mean and standard deviation from the present study and GSWP3. The statistical parameters for model evaluation are the coefficient of determination (r^2), the weighted root-mean-square error (RMSE), and the mean bias error (MBE).

		Regions of interest					
Variable	**Case**	**Global land**	**Tropical**	**Arid**	**Temperate**	**Boreal**	**Polar**
Incoming shortwave (W m^{-2})	**CAM**	186.25 ± 53.6	207.23 ± 20.68	240.05 ± 26.04	191.04 ± 30.84	137.35 ± 40.37	138.87 ± 42.24
	GSWP3	181.95 ± 52.16	213.6 ± 17.55	230.8 ± 29.65	185.58 ± 33.14	134.45 ± 27.83	128.5 ± 37.04
	r^2	0.92	0.53	0.64	0.77	0.94	0.81
	RMSE	17.94	16.02	21.00	18.22	15.39	18.07
	MBE	4.30	-6.37	9.25	5.46	2.90	10.37
Incoming longwave (W m^{-2})	**CAM**	308.81 ± 79.18	397.29 ± 15.97	335.41 ± 39.36	340.1 ± 27.96	271.7 ± 22.04	177.73 ± 62.74
	GSWP3	309.79 ± 76.79	396.4 ± 15.63	338.88 ± 34.84	338.71 ± 27.03	270.7 ± 22.44	181.84 ± 55.87
	r^2	0.99	0.90	0.94	0.92	0.86	0.98
	RMSE	9.38	5.05	10.99	7.69	8.80	12.39
	MBE	-0.99	0.89	-3.47	1.39	1.00	-4.11
Temperature of lowest atmospheric layer (K)	**CAM**	281.83 ± 18.34	297 ± 1.88	292.98 ± 6.67	289.31 ± 4.57	273.37 ± 6.63	249.73 ± 16.31
	GSWP3	282.95 ± 18.02	298.79 ± 1.88	293.99 ± 7.46	289.67 ± 4.91	273.27 ± 6.56	252.37 ± 15.35
	r^2	0.99	0.69	0.95	0.91	0.96	0.95
	RMSE	2.52	2.09	2.04	1.57	1.36	4.49
	MBE	-1.13	-1.79	-1.01	-0.35	0.11	-2.64
Specific humidity of lowest atmospheric layer (g kg^{-1})	**CAM**	6.96 ± 4.83	14.34 ± 2.1	6.44 ± 2.74	8.72 ± 2.66	3.92 ± 1.13	1.37 ± 1.45
	GSWP3	7.34 ± 5.24	15.39 ± 2.65	6.58 ± 2.65	9.32 ± 3.24	3.94 ± 1.21	1.56 ± 1.48
	r^2	0.96	0.50	0.77	0.85	0.90	0.94
	RMSE	1.36	2.21	1.38	1.49	0.41	0.42
	MBE	-0.37	-1.05	-0.14	-0.60	-0.01	-0.19
Surface pressure (hPa)	**CAM**	925.97 ± 94.86	963.35 ± 37.73	935.23 ± 65.03	943.27 ± 64.66	947.28 ± 71.53	797.89 ± 139.08
	GSWP3	925.44 ± 97.48	962.19 ± 41.08	934.6 ± 66.2	940.99 ± 69.29	947.23 ± 76.87	796.24 ± 142
	r^2	0.98	0.85	0.95	0.91	0.96	0.98
	RMSE	16.45	16.08	14.90	20.65	14.37	20.04
	MBE	0.53	1.16	0.63	2.29	0.05	1.65
Wind speed (m s^{-1})	**CAM**	5.25 ± 2.07	3.15 ± 1.31	5.38 ± 0.94	4.52 ± 1.24	5.42 ± 1.05	7.86 ± 2.72
	GSWP3	3.26 ± 1.37	2.12 ± 0.96	3.06 ± 0.92	2.97 ± 1.14	3.44 ± 1.03	4.81 ± 1.46
	r^2	0.65	0.38	0.24	0.62	0.54	0.48
	RMSE	2.39	1.51	2.52	1.77	2.13	3.60
	MBE	1.99	1.02	2.32	1.56	1.98	3.04
Precipitation rate (mm hr^{-1})	**CAM**	0.1 ± 0.1	0.23 ± 0.12	0.05 ± 0.04	0.13 ± 0.07	0.08 ± 0.04	0.05 ± 0.06
	GSWP3	0.09 ± 0.08	0.19 ± 0.09	0.03 ± 0.03	0.13 ± 0.06	0.07 ± 0.03	0.04 ± 0.04
	r^2	0.79	0.57	0.66	0.48	0.53	0.68
	RMSE	0.05	0.09	0.03	0.06	0.03	0.04
	MBE	0.02	0.04	0.02	0.01	0.01	0.01

Table S3. Evaluation of the surface radiation and energy budget components simulated by CAM and CLM against MERRA-2 for 2001-2003 for the world's land surfaces and for each climate zone. The top two rows for each variable show the grid-area weighted mean and standard deviation from the present study and MERRA-2. The statistical parameters for model evaluation are the coefficient of determination (r^2), the weighted root-mean-square error (RMSE), and the mean bias error (MBE).

		Regions of interest					
Variable	**Case**	**Global land**	**Tropical**	**Arid**	**Temperate**	**Boreal**	**Polar**
Incoming shortwave ($W\ m^{-2}$)	**CAM-CLM**	185.85 ± 54	206.8 ± 21.14	240.06 ± 26.26	190.4 ± 31.93	135.95 ± 40.55	139.4 ± 42.71
	MERRA-2	196.29 ± 59.19	225.38 ± 23.75	252.15 ± 27.63	211.25 ± 31.93	142.54 ± 39	135.4 ± 46.64
	r^2	0.93	0.42	0.67	0.73	0.95	0.91
	RMSE	20.36	25.43	20.99	28.23	11.51	13.40
	MBE	-10.44	-18.58	-12.09	-20.85	-6.59	4.00
Reflected shortwave ($W\ m^{-2}$)	**CAM-CLM**	49.08 ± 31.05	30.58 ± 4.58	60.46 ± 27.87	29.22 ± 7.33	32.73 ± 12.78	93.78 ± 32.25
	MERRA-2	46.38 ± 27.96	29.21 ± 5.83	62.98 ± 26.7	30.4 ± 7.57	29.71 ± 7.75	79.51 ± 30.93
	r^2	0.92	0.26	0.86	0.54	0.58	0.92
	RMSE	10.44	4.71	9.94	5.24	8.63	17.13
	MBE	2.70	1.37	-2.53	-1.18	3.01	14.27
Incoming longwave ($W\ m^{-2}$)	**CAM-CLM**	307.8 ± 79.7	396.95 ± 16.1	334.71 ± 39.37	339.08 ± 27.56	270.9 ± 21.82	175.13 ± 62.36
	MERRA-2	294.58 ± 76.46	387.96 ± 19.12	312.93 ± 37.65	321.79 ± 30.58	259.73 ± 20.68	169.94 ± 55.52
	r^2	0.99	0.82	0.94	0.91	0.89	0.98
	RMSE	17.60	12.12	23.85	19.48	13.79	15.17
	MBE	13.22	9.00	21.78	17.30	11.17	5.19
Emitted longwave ($W\ m^{-2}$)	**CAM-CLM**	374.32 ± 89.33	451 ± 12.96	433.69 ± 38.26	407.43 ± 27.1	324.13 ± 31.48	222.28 ± 63.27
	MERRA-2	365.55 ± 85.49	446.99 ± 11.67	417.39 ± 39.37	394.58 ± 28.46	315.46 ± 26.79	222.16 ± 58.86
	r^2	0.99	0.53	0.96	0.87	0.96	0.97
	RMSE	14.09	10.07	18.16	16.59	11.44	11.56
	MBE	8.77	4.00	16.30	12.85	8.67	0.12
Sensible heat flux ($W\ m^{-2}$)	**CAM-CLM**	32.05 ± 27.86	41.87 ± 14.22	56.22 ± 14.96	40.78 ± 14.59	19.89 ± 12.27	-9.82 ± 24.86
	MERRA-2	35.37 ± 33.06	41.44 ± 27.67	65.66 ± 18.51	44.51 ± 21.94	18.34 ± 18.32	-3.48 ± 29.89
	r^2	0.78	0.34	0.40	0.32	0.59	0.82
	RMSE	16.74	21.43	16.30	18.43	11.64	12.04
	MBE	-3.33	0.43	-9.44	-3.72	1.55	-6.34
Latent heat flux ($W\ m^{-2}$)	**CAM-CLM**	37.42 ± 29.23	80.33 ± 17.13	24.18 ± 17.52	51.66 ± 16.8	27.9 ± 10.68	7.19 ± 11.17
	MERRA-2	43.13 ± 37.3	95.02 ± 29.58	18.28 ± 16.94	63.37 ± 24.11	36.31 ± 11.53	9.03 ± 11.72
	r^2	0.81	0.42	0.38	0.38	0.43	0.64
	RMSE	18.44	26.60	14.44	22.08	13.03	7.67
	MBE	-5.71	-14.69	5.90	-11.71	-8.41	-1.84
Ground flux ($W\ m^{-2}$)	**CAM-CLM**	0.79 ± 1.43	-0.03 ± 0.12	0.24 ± 0.5	0.42 ± 0.87	2.24 ± 1.54	1.1 ± 2.03
	MERRA-2	0.14 ± 0.21	0.1 ± 0.15	0.12 ± 0.15	0.09 ± 0.18	0.26 ± 0.27	0.09 ± 0.23
	r^2	0.14	0.00	0.01	0.02	0.00	0.23

RMSE	1.53	0.23	0.53	0.92	2.52	2.21
MBE	0.65	-0.12	0.12	0.33	1.98	1.01